

# NLO QCD corrections to the production of Higgs plus two jets at the LHC <sup>☆</sup>

H. van Deurzen<sup>a</sup>, N. Greiner<sup>a</sup>, G. Luisoni<sup>a</sup>, P. Mastrolia<sup>a,b</sup>, E. Mirabella<sup>a</sup>, G. Ossola<sup>c,d</sup>, T. Peraro<sup>a</sup>,  
J. F. von Soden-Fraunhofen<sup>a</sup>, F. Tramontano<sup>e,f</sup>

<sup>a</sup>Max-Planck-Institut für Physik, Föhringer Ring 6, 80805 München, Germany

<sup>b</sup>Dipartimento di Fisica e Astronomia, Università di Padova, and INFN

Sezione di Padova, via Marzolo 8, 35131 Padova, Italy

<sup>c</sup>New York City College of Technology, City University of New York, 300 Jay Street, Brooklyn NY 11201, USA

<sup>d</sup>The Graduate School and University Center, City University of New York, 365 Fifth Avenue, New York, NY 10016, USA

<sup>e</sup>Dipartimento di Scienze Fisiche, Università degli studi di Napoli “Federico II”, I-80125 Napoli, Italy

<sup>f</sup>INFN, Sezione di Napoli, I-80125 Napoli, Italy

## Abstract

We present the calculation of the NLO QCD corrections to the associated production of a Higgs boson and two jets, in the infinite top-mass limit. We discuss the technical details of the computation and we show the numerical impact of the radiative corrections on several observables at the LHC. The results are obtained by using a fully automated framework for fixed order NLO QCD calculations based on the interplay of the packages GOSAM and SHERPA. The evaluation of the virtual corrections constitutes an application of the  $d$ -dimensional integrand-level reduction to theories with higher dimensional operators. We also present first results for the one-loop matrix elements of the partonic processes with a quark-pair in the final state, which enter the hadronic production of a Higgs boson together with three jets in the infinite top-mass approximation.

**Keywords:** QCD, Jets, NLO Computations, LHC

## 1. Introduction

The recent discovery reported by ATLAS and CMS [1, 2] indicates the existence of a new neutral boson with mass of about 125 GeV and spin different from one. At present, all measurements are consistent with the hypothesis that the new particle is the Standard Model Higgs boson. Nevertheless, further studies concerning its CP properties, spin, and couplings are mandatory to confirm its nature.

The vector boson fusion (VBF) processes can be used to study the CP properties of the new particle, and to extract its couplings with the heavy gauge bosons. The dominant background to VBF comes from Higgs plus two jet production via gluon fusion ( $Hjj$ ). The signal-over-background ratio can be improved by imposing stringent cuts on the Higgs decay products, and by requiring large rapidity separation between the two forward jets. A veto on the jet activity in the central region further reduces the impact of the background. Indeed, VBF processes are characterized by low hadronic activity, owing to the exchange of

a color-singlet in the  $t$ -channel. An accurate estimation of the efficiency of the central-jet veto requires the inclusion of the next-to-leading order (NLO) corrections to  $Hjj$  production [3, 4].

The leading order (LO) contribution to  $Hjj$  production has been computed in Refs. [5, 6]. The calculation was performed retaining the full top-mass dependence, and it showed the validity of the large top-mass approximation ( $m_t \rightarrow \infty$ ) whenever the mass of the Higgs particle and the  $p_T$  of the jets are not sensibly larger than the mass of the top quark. In the  $m_t \rightarrow \infty$  limit, the Higgs coupling to two gluons, which at LO is mediated by a top-quark loop, becomes independent of  $m_t$ . Hence, it can be described by an effective operator obtained by integrating out the top quark degrees of freedom [7]. In this approximation, the number of loops of the virtual diagrams that need to be computed is reduced by one.

In the heavy top quark limit, the inclusive Higgs boson production cross section has been computed at NLO [8, 9] and at next-to-next-to-leading order (NNLO) [10–12], showing a reduced sensitivity of the perturbative prediction to scale variations.

The implementation of final state cuts, to reduce the impact of the Standard Model background for the identification of Higgs production demands fully exclusive calculations of the theory predictions. In the  $m_t \rightarrow \infty$  limit, the NNLO corrections to Higgs production via gluon fusion have been computed fully exclusively [13–16]. These

<sup>☆</sup>DSF-03-2013, MPP-2013-36

Email addresses: hdeurzen@mpp.mpg.de (H. van Deurzen), greiner@mpp.mpg.de (N. Greiner), luisonig@mpp.mpg.de (G. Luisoni), pierpaolo.mastrolia@cern.ch (P. Mastrolia), mirabell@mpp.mpg.de (E. Mirabella), Gossola@citytech.cuny.edu (G. Ossola), peraro@mpp.mpg.de (T. Peraro), jfsoden@mpp.mpg.de (J. F. von Soden-Fraunhofen), francesco.tramontano@cern.ch (F. Tramontano)

corrections also included the contributions of  $H + 1j$  final states to NLO [17–20], and of the  $H + 2j$  final states to LO [21, 22].

The impact of the NLO QCD corrections to the  $Hjj$  production rate has been studied in Ref. [3], using the real corrections presented in Refs. [23–25] and the semi-analytic virtual corrections computed in Refs. [26, 27]. A great effort has been devoted to the analytic computation of the one-loop helicity amplitudes involving Higgs plus four partons, using on-shell and generalized unitarity methods [28–34]. The resulting compact expressions have been implemented in MCFM [4], which has been used to obtain matched NLO plus shower predictions within the POWHEG box framework [35].

In this letter we present an independent computation of the NLO contributions to Higgs plus two jets production at the LHC in the large top-mass limit. These results have been obtained by using a fully automated framework for fixed order NLO QCD calculations, which interfaces via the Binoth Les Houches Accord (BLHA) [36] the GOSAM package [37], for the generation and computation of the virtual amplitudes, with the SHERPA package [38], for the computation of the real amplitudes and the Monte Carlo integration over phase space. Details of the GOSAM - SHERPA interface, together with a selection of ready-to-use process packages, can be found in [39, 40]. Moreover, the evaluation of the virtual corrections for a model described by an effective Lagrangian constitutes an application of the  $d$ -dimensional integrand reduction [41–46] to theories with higher dimensional operators [47]. In Section 2 we present the computational setup, whereas results on  $pp \rightarrow Hjj$  at the LHC are discussed in Section 3.

Finally, we explore the possibility of extending our framework to consider the production of a Higgs boson plus three jets ( $Hjjj$ ). We generate codes for the virtual corrections to the partonic processes with a quark-pair in the final state. We show the corresponding results in Section 4.

Appendix A contains the definitions of the Feynman rules for the direct interaction between the Higgs boson and gluons via effective couplings. In Appendix B, we show a property of the highest-rank terms of the one-loop integrands stemming from those effective rules. We close this communication by collecting, in Appendix C and Appendix D, the numerical results of the virtual matrix elements, evaluated in non-exceptional phase space points, for  $H + 2j$  and  $H + 3j$  final states, respectively.

## 2. Computational setup

We compute Higgs plus two jets production through gluon fusion in the large top-mass limit ( $m_t \rightarrow \infty$ ). In this limit, the Higgs-gluon coupling is described by the effective local interaction [7]

$$\mathcal{L} = -\frac{g_{\text{eff}}}{4} H \text{tr}(G_{\mu\nu} G^{\mu\nu}). \quad (1)$$

In the  $\overline{\text{MS}}$  scheme, the coefficient  $g_{\text{eff}}$  reads [8, 9]

$$g_{\text{eff}} = -\frac{\alpha_s}{3\pi v} \left(1 + \frac{11}{4\pi} \alpha_s\right) + \mathcal{O}(\alpha_s^3), \quad (2)$$

in terms of the Higgs vacuum expectation value  $v$ . The operator (1) leads to new Feynman rules involving the Higgs field and up to four gluons. They are collected in Appendix A.

Next-to-leading order corrections to cross sections require the evaluation of virtual and real emission contributions. For the computation of the virtual corrections we use a code generated by the program package GOSAM, which combines automated diagram generation and algebraic manipulation [48–51] with integrand-level reduction techniques [41–43, 52–54]. More specifically, the virtual corrections are evaluated using the  $d$ -dimensional integrand-level decomposition implemented in the SAMURAI library [45], which allows for the combined determination of both cut-constructible and rational terms at once. Moreover, the presence of effective couplings in the Lagrangian requires an extended version [47] of the integrand-level reduction, of which the present calculation is a first application. After the reduction, all relevant scalar (master) integrals are computed by means of QCDLOOP [55, 56], ONELOOP [57], or GOLEM95C [58].

For the calculation of tree-level contributions we use SHERPA [38], which computes the LO and the real radiation matrix elements [59], regularizes the IR and collinear singularities using the Catani-Seymour dipole formalism [60], and carries out the phase space integrations as well.

The code that evaluates the virtual corrections is generated by GOSAM and linked to SHERPA via the Binoth-Les-Houches Accord (BLHA) [36] interface. This interface allows to generate the code in a fully automated way by a system of order and contract files containing the amplitudes requested by SHERPA. Furthermore, it allows for a direct communication between the two codes at running time, when SHERPA steers the integration by calling the external code which computes the virtual amplitude. A detailed description of this interface is beyond the scope of this paper and will be presented elsewhere [39].

For  $Hjj$  production, the partonic processes in the contract file are:

$$\begin{aligned} qq &\rightarrow Hqq, & q\bar{q} &\rightarrow Hq\bar{q}, \\ q\bar{q} &\rightarrow Hgg, & q\bar{q} &\rightarrow Hq'q', \\ qq' &\rightarrow Hqq', & qq &\rightarrow Hgq, \\ \bar{q}q &\rightarrow Hq\bar{q}, & \bar{q}q' &\rightarrow Hq'\bar{q}, \\ gq &\rightarrow Hgq, & gg &\rightarrow Hq\bar{q}, \\ gg &\rightarrow Hgg. \end{aligned} \quad (3)$$

These processes are not independent, as they can be related by crossing and/or by relabeling. GOSAM identifies

and generates the following minimal set of processes

$$\begin{aligned} gg &\rightarrow Hgg, & gg &\rightarrow Hq\bar{q}, \\ q\bar{q} &\rightarrow Hq\bar{q}, & q\bar{q} &\rightarrow Hq'\bar{q}'. \end{aligned} \quad (4)$$

The other processes are obtained by performing the appropriate symmetry transformation.

The ultraviolet (UV), the infrared, and the collinear singularities are regularized using dimensional reduction (DRED). UV divergences have been renormalized in the  $\overline{\text{MS}}$  scheme. In the case of LO [NLO] contributions we describe the running of the strong coupling constant with one-loop [two-loop] accuracy, decoupling the top quark from the running.

The effective  $Hgg$  coupling, see Appendix A, leads to integrands that may exhibit numerators with rank  $r$  larger than the number  $n$  of the denominators, i.e.  $r \leq n+1$ . In general, for these cases, the parametrization of the residues at the multiple-cut has to be extended as discussed in Ref. [47]. As a consequence, the decomposition of any one-loop  $n$ -point amplitude in terms of master integrals (MIs) acquires new contributions, reading as,

$$\mathcal{M}_n^{\text{one-loop}} = \mathcal{A}_n + \delta\mathcal{A}_n. \quad (5)$$

The term  $\mathcal{A}_n$  corresponds to the standard decomposition for the case of a renormalizable theory ( $r \leq n$ ), while the additional contribution  $\delta\mathcal{A}_n$  enters whenever  $r \leq n+1$ . Their actual expressions can be found in Eqs. (2.16) and (6.11) of [47].

The extended integrand decomposition has been implemented in the SAMURAI library. In particular, the coefficients multiplying the MIs appearing in  $\mathcal{A}_n$  and  $\delta\mathcal{A}_n$  are computed by using the discrete Fourier transform as described in Refs. [45, 53].

In the case of Higgs plus jets production, higher rank numerators arise from diagrams where the Higgs boson is attached to a pure gluonic loop. However, as shown in Appendix B, the rank- $(n+1)$  terms of an  $n$ -point integrand are proportional to the loop momentum squared,  $q^2$ , which simplifies against a denominator. Therefore, they generate  $(n-1)$ -point integrands with rank  $r = n-1$ . Consequently, the coefficients of the MIs in  $\delta\mathcal{A}_n$  have to vanish identically, as explicitly verified. Since  $\delta\mathcal{A}_n$  in Eq. (5) does not play any role, the integrand reduction can be also performed with the current public version of SAMURAI, which does not contain the extended decomposition - hence, implying a lighter reduction, with fewer coefficients involved.

We remark that, within the integrand reduction algorithm, it is possible to benefit immediately from the presence of powers of  $q^2$  in the numerators, without any algebraic cost: the contribution of those terms is automatically taken into account by the integrand reconstruction of the subdiagrams (because they give no contribution on the corresponding massless cut). On the contrary, within a tensor reduction algorithm, these terms would cancel only after the algebraic manipulation of the integrand.

The numerical values of the one-loop amplitudes of the processes (4) in a non-exceptional phase space point are collected in Appendix C. The values of the double and the single poles conform to the universal singular behavior of dimensionally regulated one-loop amplitudes [61–65]. After appropriate crossing to the  $H \rightarrow 4$ -parton decay kinematics, we compared our results with the ones presented in Table I of Ref. [26], finding excellent agreement. Furthermore, converting our results for the  $Hjj$ -production channels from DRED to the 't Hooft-Veltman scheme, we are in perfect agreement with the most recent version of MCFM (v6.4).

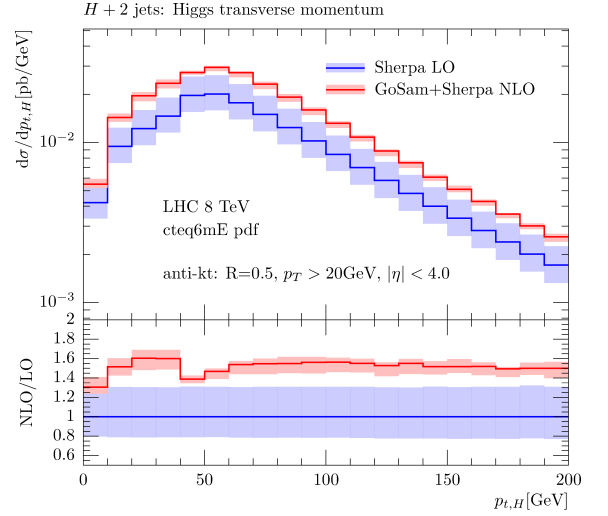


Figure 1: Transverse momentum  $p_T$  of the Higgs boson.

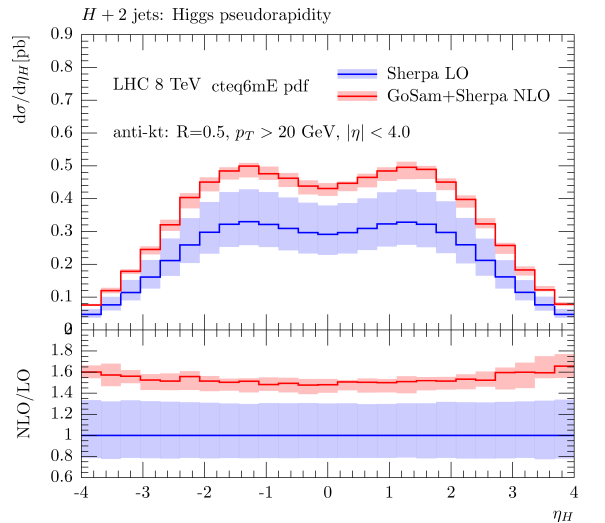


Figure 2: Pseudorapidity  $\eta$  of the Higgs boson.

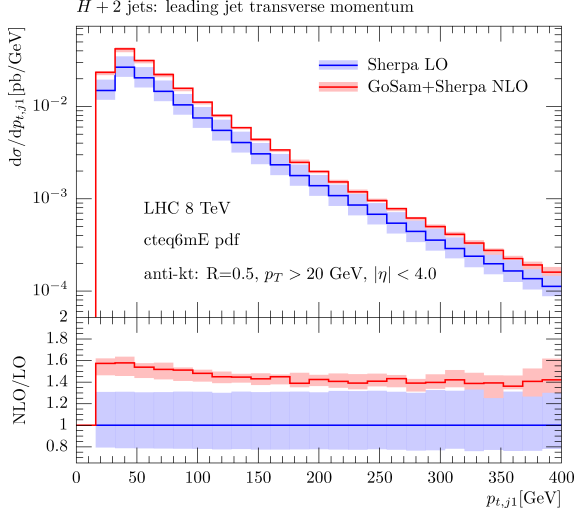


Figure 3: Transverse momentum  $p_T$  of the first jet.

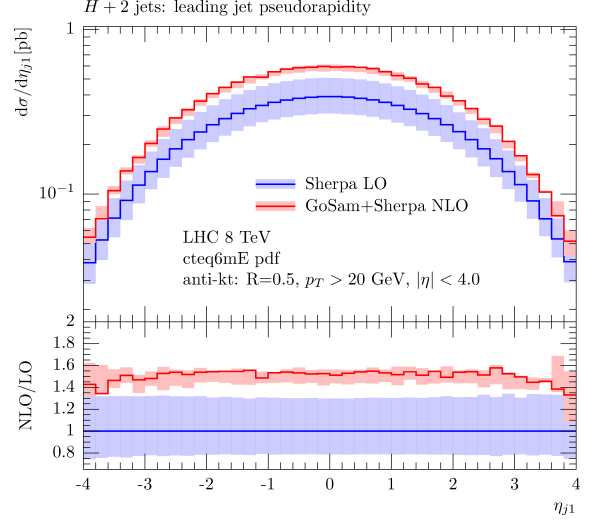


Figure 5: Pseudorapidity  $\eta$  of the first jet.

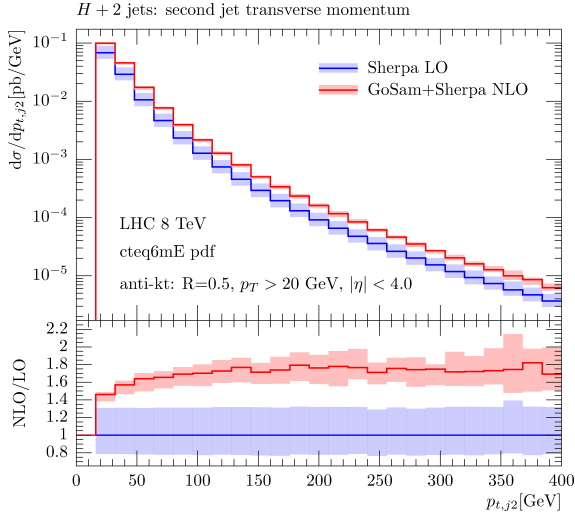


Figure 4: Transverse momentum  $p_T$  of the second jet.

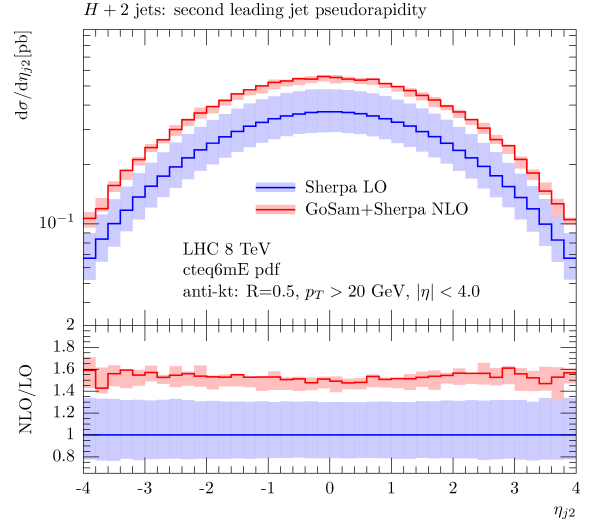


Figure 6: Pseudorapidity  $\eta$  of the second jet.

### 3. Numerical results for $pp \rightarrow Hjj$

In this section we present a selection of phenomenological results for proton-proton collisions at the LHC at  $\sqrt{s} = 8$  TeV, as a sample of the results that can be easily obtained with the GoSAM-SHERPA automated setup [37–40]. A more complete analysis of Higgs production in gluon fusion, which merges several multiplicities [66] and employs the code for the virtual matrix elements of  $Hjj$  presented here, is going to be discussed in [67].

The results shown in this section are obtained using the parameters listed below:

$$\begin{aligned} M_H &= 125 \text{ GeV}, & G_F &= 1.16639 \cdot 10^{-5} \text{ GeV}^{-2}, \\ \alpha_s^{\text{LO}}(M_Z) &= 0.129783, & \alpha_s^{\text{NLO}}(M_Z) &= 0.117981, \\ v^2 &= \frac{1}{\sqrt{2}G_F}. \end{aligned} \quad (6)$$

We use the CTEQ6L1 and CTEQ6mE [68] parton distribution functions (PDF) for the LO and NLO, respectively. The value of the strong coupling at the scale  $\mu$  is taken from the PDF set starting from the initial values in Eq. (6). The jets are clustered by using the anti- $k_T$  algorithm provided by the FASTJET package [69–71] with the following setup:

$$p_{t,j} \geq 20 \text{ GeV}, \quad |\eta_j| \leq 4.0, \quad R = 0.5. \quad (7)$$

The Higgs boson is treated as a stable on-shell particle, without including any decay mode. To fix the factorization and the renormalization scale we define

$$\hat{H}_t = \sqrt{M_H^2 + p_{t,H}^2} + \sum_j p_{t,j}, \quad (8)$$

where  $p_{t,H}$  and  $p_{t,j}$  are the transverse momenta of the Higgs boson and the jets. The nominal value for the two

scales is defined as

$$\mu = \mu_R = \mu_F = \hat{H}_t, \quad (9)$$

whereas theoretical uncertainties are assessed by varying simultaneously the factorization and renormalization scales in the range

$$\frac{1}{2}\hat{H}_t < \mu < 2\hat{H}_t. \quad (10)$$

The error is estimated by taking the envelope of the resulting distributions at the different scales.

### 3.1. Results

Within our framework, we find the following total cross sections for the process  $pp \rightarrow Hjj$  in gluon fusion:

$$\sigma_{\text{LO}}[\text{pb}] = 1.90^{+0.58}_{-0.41},$$

$$\sigma_{\text{NLO}}[\text{pb}] = 2.90^{+0.05}_{-0.20},$$

where the error is obtained by varying the renormalization and factorization scales as given in Eq. (9). The LO distributions have been computed using  $2.5 \times 10^7$  phase space points, whereas all NLO distributions have been obtained using  $4.0 \times 10^6$  phase space points for the Born and the virtual corrections and  $5.0 \times 10^8$  points for the real radiation for each scale.

In Figs. 1 and 2, we present the distribution of the transverse momentum  $p_T$  of the Higgs boson and its pseudorapidity  $\eta$ , respectively. Both of them show a K-factor between the LO and the NLO distribution of about 1.5–1.6, which is almost flat over a large fraction of kinematical range. Furthermore both plots show a decrease of the scale uncertainty of about 50%. Figures 3 and 4 display the transverse momentum of the first and second jet, whereas their pseudorapidities are shown in Figs. 5 and 6. The previous considerations are also true for these latter plots. For the transverse momentum distributions, however, we observe a slight change of shapes. In the case of the leading jet, increasing the  $p_T$ , the K-factor decreases from 1.6 to 1.4; while for the second leading jet, it increases from 1.4 to 1.6.

## 4. Virtual corrections to $pp \rightarrow Hjjj$

We explore the possibility of extending our framework to the production of a Higgs boson plus three jets at NLO.

The independent partonic processes contributing to  $Hjjj$  can be obtained by adding one extra gluon to the final state of the processes listed in Eq.(4). Accordingly, we generate the codes for the virtual corrections to the partonic processes with a quark-pair in the final state,

$$gg \rightarrow Hq\bar{q}g, \quad q\bar{q} \rightarrow Hq\bar{q}g, \quad q\bar{q} \rightarrow Hq'\bar{q}'g. \quad (11)$$

The missing channel  $gg \rightarrow Hggg$ , together with the phase space integration, will be discussed in a successive study.

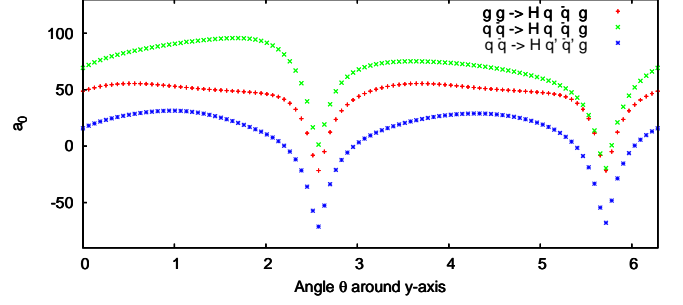


Figure 7: Finite-term of the virtual matrix-elements for  $gg \rightarrow Hq\bar{q}g$  (red),  $q\bar{q} \rightarrow Hq\bar{q}g$  (green),  $q\bar{q} \rightarrow Hq'\bar{q}'g$  (blue).

We compute, for the first time, the virtual matrix elements for the three subprocesses listed above, and show their results along a certain one-dimensional curve in the space of final state momenta. We take the initial partons to have momentum  $p_1$  and  $p_2$ , whose 3-momenta lie along the  $z$ -axis, and choose an arbitrary point for the final state momenta  $\{p_3, p_4, p_5, p_6\}$ . For simplicity, we start with the same phase space point used in the Appendix D (see Table D.4). Then, we create new momentum configurations by rotating the final state through an angle  $\theta$  about the  $y$ -axis. Figure 7 displays the behavior of the finite part  $a_0$  of the individual  $2 \rightarrow 4$  amplitudes defined as

$$\frac{2\Re\{\mathcal{M}^{\text{tree-level}*}\mathcal{M}^{\text{one-loop}}\}}{(4\pi\alpha_s)|\mathcal{M}^{\text{tree-level}}|^2} \equiv \frac{a_{-2}}{\epsilon^2} + \frac{a_{-1}}{\epsilon} + a_0, \quad (12)$$

when the final external momenta are rotated from  $\theta = 0$  to  $\theta = 2\pi$ . The plots are obtained by sampling over 100 points.

Numerical values for the one-loop amplitudes of the processes listed in (11) are collected in Appendix D.

Also in this case we verify that the values of the double and the single poles conform to the universal singular behavior of dimensionally regulated one-loop amplitudes [65].

## 5. Conclusions

We presented the calculation of the associated production of a Higgs boson and two jets,  $pp \rightarrow Hjj$ , at NLO in QCD, employing the infinite top-mass approximation.

The results were obtained by using a fully automated framework for fixed order NLO QCD calculations based on the interplay of the packages GOSAM and SHERPA, interfaced through the BLHA standards. We discussed the technical aspects of the computation, and showed the numerical impact of the radiative corrections on the distribution of the transverse momentum of the Higgs boson and its pseudorapidity, as well as of the transverse momentum and pseudorapidity of the leading and second leading jet. All plots show a K-factor between the LO and the NLO

distributions of about 1.5, over a large fraction of kinematical range, and a decrease of the scale uncertainty of about 50%.

The evaluation of the virtual corrections constitutes an application of the  $d$ -dimensional integrand reduction to theories with higher dimensional operators.

Finally, as an initial step towards the evaluation of  $pp \rightarrow Hjjj$  at NLO, we presented first results for the one-loop matrix elements of the partonic processes with a quark-pair in the final state.

## Acknowledgements

We thank the SHERPA collaboration for encouraging and stimulating discussions and feedback on the manuscript. We also would like to thank Thomas Hahn for his technical support while structuring the computing resources needed by our codes, and Joscha Reichel for feedback on the extended-rank version of SAMURAI.

The work of H.v.D., G.L., P.M., and T.P. was supported by the Alexander von Humboldt Foundation, in the framework of the Sofja Kovaleskaja Award Project “Advanced Mathematical Methods for Particle Physics”, endowed by the German Federal Ministry of Education and Research.

G.O. was supported in part by the National Science Foundation under Grant PHY-1068550.

H.v.D. and G.L. thank the Center for Theoretical Physics of New York City College of Technology for hospitality during the final stages of this project.

The Feynman diagrams present in this paper are drawn using FEYNARTS [72].

## Appendix A. Effective Higgs-gluon vertices

The operator  $\mathcal{L}$  in Eq. (1) describes the gluon-Higgs interaction in the large top-mass limit and leads to the following set of Feynman rules:

$$\begin{aligned}
 \text{Diagram 1: } H \text{ (dashed line) connected to a gluon loop (two wavy lines). The top vertex is labeled } g_1 \text{ and the bottom vertex is labeled } g_2. &= -ig_{\text{eff}} \mathcal{F}_{c_1, c_2}^{\mu_1 \mu_2} \\
 \text{Diagram 2: } H \text{ (dashed line) connected to a gluon loop (two wavy lines). The top vertex is labeled } g_1, \text{ the bottom-left vertex is labeled } g_2, \text{ and the bottom-right vertex is labeled } g_3. &= g_{\text{eff}} g_s \mathcal{F}_{c_1, c_2, c_3}^{\mu_1 \mu_2 \mu_3} \\
 \text{Diagram 3: } H \text{ (dashed line) connected to a gluon loop (two wavy lines). The top-left vertex is labeled } g_1, \text{ the top-right vertex is labeled } g_2, \text{ the bottom-left vertex is labeled } g_3, \text{ and the bottom-right vertex is labeled } g_4. &= ig_{\text{eff}} g_s^2 \mathcal{F}_{c_1, c_2, c_3, c_4}^{\mu_1 \mu_2 \mu_3 \mu_4}
 \end{aligned}$$

where we define

$$\begin{aligned}
 \mathcal{F}_{c_1, c_2}^{\mu_1 \mu_2} &= \delta_{c_1 c_2} (p_1^{\mu_2} p_2^{\mu_1} - p_1 \cdot p_2 g^{\mu_1 \mu_2}), \\
 \mathcal{F}_{c_1, c_2, c_3}^{\mu_1 \mu_2 \mu_3} &= f_{c_1 c_2 c_3} [g^{\mu_1 \mu_2} (p_1^{\mu_3} - p_2^{\mu_3}) \\
 &\quad + g^{\mu_2 \mu_3} (p_2^{\mu_1} - p_3^{\mu_1}) \\
 &\quad + g^{\mu_3 \mu_1} (p_3^{\mu_2} - p_1^{\mu_2})], \\
 \mathcal{F}_{c_1, c_2, c_3, c_4}^{\mu_1 \mu_2 \mu_3 \mu_4} &= f_{c_1 c_2 i} f_{c_3 c_4 i} [g^{\mu_1 \mu_4} g^{\mu_2 \mu_3} - g^{\mu_1 \mu_3} g^{\mu_2 \mu_4}] \\
 &\quad + f_{c_1 c_3 i} f_{c_2 c_4 i} [g^{\mu_1 \mu_4} g^{\mu_2 \mu_3} - g^{\mu_1 \mu_2} g^{\mu_3 \mu_4}] \\
 &\quad + f_{c_1 c_4 i} f_{c_2 c_3 i} [g^{\mu_1 \mu_3} g^{\mu_2 \mu_4} - g^{\mu_1 \mu_2} g^{\mu_3 \mu_4}].
 \end{aligned} \tag{A.1}$$

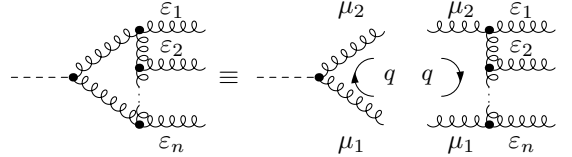
In Eq. (A.1) sum over repeated indices is understood.

## Appendix B. Higher-rank integrands

Higher-rank integrands, i.e. integrands where the powers of loop momenta in the numerator is higher than the numbers of denominators, are present in diagrams with a Higgs boson coupled to a purely gluonic loop involving only three-gluon vertices. The generic numerator  $\Gamma^{\varepsilon_1 \dots \varepsilon_n}$  of a  $(n+1)$ -denominator one-loop diagram can be written as

$$\Gamma^{\varepsilon_1 \dots \varepsilon_n} \equiv \mathcal{F}_{\mu_1 \mu_2} \mathcal{G}^{\mu_1 \mu_2 \varepsilon_1 \dots \varepsilon_n}, \tag{B.1}$$

where  $\mathcal{F}_{\mu_1 \mu_2}$  is the  $Hgg$  vertex defined in Eq. (A.1), and  $\mathcal{G}^{\mu_1 \mu_2 \varepsilon_1 \dots \varepsilon_n}$  is the numerator of an  $(n+2)$ -gluon tree-level diagram, which can be represented by



We are interested in the leading behaviour in  $q$  of  $\Gamma^{\varepsilon_1 \dots \varepsilon_n}$ , and we want to show that the highest-rank terms, with rank  $r = n + 2$ , are proportional to the loop momentum squared,  $q^2$ . In order to show it, we neglect all external momenta and all the terms proportional to  $q^2$ .

From Eq. (A.1), one trivially has

$$\mathcal{F}_{\mu_1 \mu_2} = q_{\mu_1} q_{\mu_2} + \mathcal{O}(q^2), \tag{B.2}$$

while the generic tensor structure of  $\mathcal{G}^{\mu_1 \mu_2 \varepsilon_1 \dots \varepsilon_n}$  is

$$\begin{aligned}
 \mathcal{G}^{\mu_1 \mu_2 \varepsilon_1 \dots \varepsilon_n} &= q^{\mu_1} \mathcal{T}_1^{\mu_2 \varepsilon_1 \dots \varepsilon_n} + q^{\mu_2} \mathcal{T}_2^{\mu_1 \varepsilon_1 \dots \varepsilon_n} + \\
 &\quad + g^{\mu_1 \mu_2} \mathcal{T}_g^{\varepsilon_1 \dots \varepsilon_n} + \mathcal{O}(q^2),
 \end{aligned} \tag{B.3}$$

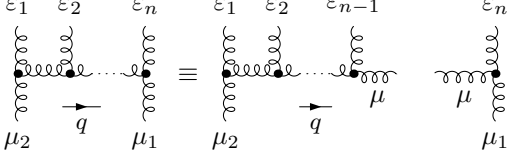
where  $\mathcal{T}_1, \mathcal{T}_2$ , and  $\mathcal{T}_g$  are tensors which may depend on  $q$  as well. Indeed Eq. (B.3) is fulfilled for  $n = 0, 1$ ,

$$\begin{aligned}
 \mathcal{G}^{\mu_1 \mu_2} &= g^{\mu_1 \mu_2} \\
 \mathcal{G}^{\mu_1 \mu_2 \varepsilon_1} &= g^{\mu_1 \varepsilon_1} q^{\mu_2} + g^{\mu_2 \varepsilon_1} q^{\mu_1} - 2g^{\mu_2 \mu_1} q^{\varepsilon_1},
 \end{aligned} \tag{B.4}$$

while for  $n > 1$  it can be proven by induction over  $n$  by using

$$\mathcal{G}^{\mu_1 \mu_2 \varepsilon_1 \dots \varepsilon_n} = \mathcal{G}_\mu^{\mu_2 \varepsilon_1 \dots \varepsilon_{n-1}} \mathcal{G}^{\mu_1 \mu \varepsilon_n}, \quad (\text{B.5})$$

that is



Combining Eq. (B.2) and Eq. (B.3), it is easy to realize that each rank- $(n+2)$  term of an  $n+1$ -denominator diagram  $\Gamma^{\varepsilon_1 \dots \varepsilon_n}$  is proportional to  $q^2$ . The factor  $q^2$  simplifies against one denominator leading to a rank  $n$  numerator of an  $n$ -denominator integrand.

### Appendix C. Benchmark points for $pp \rightarrow Hjj$

In this appendix we provide numerical results for the renormalized virtual contributions to the processes (4), in correspondence with the phase space point in Table C.1. The parameters can be read from Eqs. (6), while the renormalization and factorization scales are set to the Higgs mass value. The assignment of the momenta proceeds as follows

$$\begin{aligned} g(p_1) g(p_2) &\rightarrow H(p_3) g(p_4) g(p_5), \\ g(p_1) g(p_2) &\rightarrow H(p_3) q(p_4) \bar{q}(p_5), \\ q(p_1) \bar{q}(p_2) &\rightarrow H(p_3) q(p_4) \bar{q}(p_5), \\ q(p_1) \bar{q}(p_2) &\rightarrow H(p_3) q'(p_4) \bar{q}'(p_5). \end{aligned} \quad (\text{C.1})$$

The results are collected in Table C.2 and are computed using DRED. In the second column of the table we provide the LO squared amplitude,

$$c_0 \equiv \frac{|\mathcal{M}^{\text{tree-level}}|^2}{(4\pi\alpha_s)^2 g_{\text{eff}}^2}, \quad (\text{C.2})$$

and the coefficients  $a_i$  defined in Eq. (12). As a check on the reconstruction of the renormalized poles, in the last column we show the values of  $a_{-1}$  and  $a_{-2}$  obtained by the universal singular behavior of the dimensionally regularized one-loop amplitudes [65].

### Appendix D. Benchmark points for $pp \rightarrow Hjjj$

In this appendix we collect first numerical results for the renormalized virtual contributions to

$$\begin{aligned} g(p_1) g(p_2) &\rightarrow H(p_3) q(p_4) \bar{q}(p_5) g(p_6), \\ q(p_1) \bar{q}(p_2) &\rightarrow H(p_3) q(p_4) \bar{q}(p_5) g(p_6), \\ q(p_1) \bar{q}(p_2) &\rightarrow H(p_3) q'(p_4) \bar{q}'(p_5) g(p_6). \end{aligned} \quad (\text{D.1})$$

$gg \rightarrow Hgg$			
$c_0$	0.1507218951429643	$\cdot 10^{-3}$	
$a_0$	59.8657965614009		
$a_{-1}$	-26.4694115468536	-26.46941154671207	
$a_{-2}$	-12.000000000000001	-12.000000000000000	
$gg \rightarrow Hq\bar{q}$			
$c_0$	0.5677813961826772	$\cdot 10^{-6}$	
$a_0$	66.6635142370683		
$a_{-1}$	-16.5816633315627	-16.58166333155405	
$a_{-2}$	-8.666666666666669	-8.666666666666668	
$q\bar{q} \rightarrow Hq\bar{q}$			
$c_0$	0.1099527895267439	$\cdot 10^{-5}$	
$a_0$	88.2959834057198		
$a_{-1}$	-10.9673755313443	-10.96737553134440	
$a_{-2}$	-5.333333333333332	-5.333333333333334	
$q\bar{q} \rightarrow Hq'\bar{q}'$			
$c_0$	0.1011096724203529	$\cdot 10^{-6}$	
$a_0$	33.9521626734153		
$a_{-1}$	-13.8649292834138	-13.86492928341388	
$a_{-2}$	-5.333333333333334	-5.333333333333334	

Table C.2: Numerical results for the processes listed in Eq. (C.1)

$gg \rightarrow Hq\bar{q}g$			
$b_0$	0.6309159660038877	$\cdot 10^{-4}$	
$a_0$	48.68424097859422		
$a_{-1}$	-36.08277727147958	-36.08277728199094	
$a_{-2}$	-11.666666666667209	-11.666666666666667	
$q\bar{q} \rightarrow Hq\bar{q}g$			
$b_0$	0.3609139855530763	$\cdot 10^{-4}$	
$a_0$	69.32351140490162		
$a_{-1}$	-29.98862932963380	-29.98862932963629	
$a_{-2}$	-8.333333333333339	-8.333333333333334	
$q\bar{q} \rightarrow Hq'\bar{q}'g$			
$b_0$	0.2687990772405433	$\cdot 10^{-5}$	
$a_0$	15.79262767177915		
$a_{-1}$	-32.35320587070861	-32.35320587073038	
$a_{-2}$	-8.333333333333398	-8.333333333333332	

Table D.3: Numerical results for the processes listed in Eq. (D.1)

The results, collected in Table D.3, have been computed using the parameters in Eqs. (6), with the renormalization and factorization scales set to the Higgs mass value, and choosing the phase space point given in Table D.4. In particular, in the second column of Table D.3, we provide

particle	$E$	$p_x$	$p_y$	$p_z$
$p_1$	250.00000000000000	0.0000000000000000	0.0000000000000000	250.00000000000000
$p_2$	250.00000000000000	0.0000000000000000	0.0000000000000000	-250.00000000000000
$p_3$	143.67785106160801	51.663364918413812	-22.547134012261804	42.905108772983255
$p_4$	190.20318863787611	-153.36110830475005	-108.23578590696623	-30.702411577195452
$p_5$	166.11896030051594	101.69774338633616	130.78291991922802	-12.202697195787838

Table C.1: Benchmark phase space point for Higgs plus two jets production

particle	$E$	$p_x$	$p_y$	$p_z$
$p_1$	250.00000000000000	0.0000000000000000	0.0000000000000000	250.00000000000000
$p_2$	250.00000000000000	0.0000000000000000	0.0000000000000000	-250.00000000000000
$p_3$	131.06896655823209	27.707264814722667	-13.235482900394146	24.722529472591685
$p_4$	164.74420140597425	-129.37584098675183	-79.219260486951597	-64.240582451932028
$p_5$	117.02953632773803	54.480516624273569	97.990504664150677	-33.550658370629378
$p_6$	87.157295708055642	47.188059547755266	-5.5357612768047906	73.068711349969661

Table D.4: Benchmark phase space point for Higgs plus three jets production

the quantity  $b_0$ ,

$$b_0 \equiv \frac{|\mathcal{M}^{\text{tree-level}}|^2}{(4\pi\alpha_s)^3 g_{\text{eff}}^2}, \quad (\text{D.2})$$

and the coefficients  $a_i$  defined in Eq. (12). In the third column we show the values of  $a_{-1}$  and  $a_{-2}$  obtained from the universal singular behavior of one-loop amplitudes.

## References

- [1] **ATLAS Collaboration** Collaboration, G. Aad *et al.*, “Observation of a new particle in the search for the Standard Model Higgs boson with the ATLAS detector at the LHC,” *Phys.Lett.* **B716** (2012) 1–29, 1207.7214.
- [2] **CMS Collaboration** Collaboration, S. Chatrchyan *et al.*, “Observation of a new boson at a mass of 125 GeV with the CMS experiment at the LHC,” *Phys.Lett.* **B716** (2012) 30–61, 1207.7235.
- [3] J. M. Campbell, R. K. Ellis, and G. Zanderighi, “Next-to-Leading order Higgs + 2 jet production via gluon fusion,” *JHEP* **0610** (2006) 028, hep-ph/0608194.
- [4] J. M. Campbell, R. Ellis, and C. Williams, “Hadronic production of a Higgs boson and two jets at next-to-leading order,” *Phys.Rev.* **D81** (2010) 074023, 1001.4495.
- [5] V. Del Duca, W. Kilgore, C. Oleari, C. Schmidt, and D. Zeppenfeld, “Higgs + 2 jets via gluon fusion,” *Phys.Rev.Lett.* **87** (2001) 122001, hep-ph/0105129.
- [6] V. Del Duca, W. Kilgore, C. Oleari, C. Schmidt, and D. Zeppenfeld, “Gluon fusion contributions to H + 2 jet production,” *Nucl.Phys.* **B616** (2001) 367–399, hep-ph/0108030.
- [7] F. Wilczek, “Decays of Heavy Vector Mesons Into Higgs Particles,” *Phys.Rev.Lett.* **39** (1977) 1304.
- [8] S. Dawson, “Radiative corrections to Higgs boson production,” *Nucl.Phys.* **B359** (1991) 283–300.
- [9] A. Djouadi, M. Spira, and P. Zerwas, “Production of Higgs bosons in proton colliders: QCD corrections,” *Phys.Lett.* **B264** (1991) 440–446.
- [10] R. V. Harlander and W. B. Kilgore, “Next-to-next-to-leading order Higgs production at hadron colliders,” *Phys.Rev.Lett.* **88** (2002) 201801, hep-ph/0201206.
- [11] C. Anastasiou and K. Melnikov, “Higgs boson production at hadron colliders in NNLO QCD,” *Nucl.Phys.* **B646** (2002) 220–256, hep-ph/0207004.
- [12] V. Ravindran, J. Smith, and W. L. van Neerven, “NNLO corrections to the total cross-section for Higgs boson production in hadron hadron collisions,” *Nucl.Phys.* **B665** (2003) 325–366, hep-ph/0302135.
- [13] C. Anastasiou, K. Melnikov, and F. Petriello, “Fully differential Higgs boson production and the di-photon signal through next-to-next-to-leading order,” *Nucl.Phys.* **B724** (2005) 197–246, hep-ph/0501130.
- [14] C. Anastasiou, G. Dissertori, and F. Stockli, “NNLO QCD predictions for the  $H \rightarrow WW \rightarrow l\nu l\nu$  signal at the LHC,” *JHEP* **0709** (2007) 018, 0707.2373.
- [15] S. Catani and M. Grazzini, “An NNLO subtraction formalism in hadron collisions and its application to Higgs boson production at the LHC,” *Phys.Rev.Lett.* **98** (2007) 222002, hep-ph/0703012.
- [16] M. Grazzini, “NNLO predictions for the Higgs boson signal in the  $H \rightarrow WW \rightarrow l\nu l\nu$  and  $H \rightarrow ZZ \rightarrow 4l$  decay channels,” *JHEP* **0802** (2008) 043, 0801.3232.
- [17] C. R. Schmidt, “ $H \rightarrow g g g$  ( $g q$  anti- $q$ ) at two loops in the large  $M(t)$  limit,” *Phys.Lett.* **B413** (1997) 391–395, hep-ph/9707448.
- [18] D. de Florian, M. Grazzini, and Z. Kunszt, “Higgs production with large transverse momentum in hadronic collisions at next-to-leading order,” *Phys.Rev.Lett.* **82** (1999) 5209–5212, hep-ph/9902483.
- [19] V. Ravindran, J. Smith, and W. Van Neerven, “Next-to-leading order QCD corrections to differential distributions of Higgs boson production in hadron hadron collisions,” *Nucl.Phys.* **B634** (2002) 247–290, hep-ph/0201114.
- [20] C. J. Glosser and C. R. Schmidt, “Next-to-leading corrections to the Higgs boson transverse momentum spectrum in gluon fusion,” *JHEP* **0212** (2002) 016, hep-ph/0209248.
- [21] S. Dawson and R. Kauffman, “Higgs boson plus multi - jet rates at the SSC,” *Phys.Rev.Lett.* **68** (1992) 2273–2276.
- [22] R. P. Kauffman, S. V. Desai, and D. Risal, “Production of a Higgs boson plus two jets in hadronic collisions,” *Phys.Rev.* **D55** (1997) 4005–4015, hep-ph/9610541.
- [23] V. Del Duca, A. Frizzo, and F. Maltoni, “Higgs boson production in association with three jets,” *JHEP* **0405** (2004) 064, hep-ph/0404013.
- [24] L. J. Dixon, E. N. Glover, and V. V. Khoze, “MHV rules for Higgs plus multi-gluon amplitudes,” *JHEP* **0412** (2004) 015, hep-th/0411092.
- [25] S. Badger, E. N. Glover, and V. V. Khoze, “MHV rules for Higgs plus multi-parton amplitudes,” *JHEP* **0503** (2005) 023, hep-th/0412275.
- [26] R. K. Ellis, W. Giele, and G. Zanderighi, “Virtual QCD



- corrections to Higgs boson plus four parton processes,” *Phys.Rev.* **D72** (2005) 054018, [hep-ph/0506196](#).
- [27] R. K. Ellis, W. Giele, and G. Zanderighi, “Semi-numerical evaluation of one-loop corrections,” *Phys.Rev.* **D73** (2006) 014027, [hep-ph/0508308](#).
- [28] C. F. Berger, V. Del Duca, and L. J. Dixon, “Recursive Construction of Higgs-Plus-Multiparton Loop Amplitudes: The Last of the Phi-nite Loop Amplitudes,” *Phys.Rev.* **D74** (2006) 094021, [hep-ph/0608180](#).
- [29] S. Badger and E. N. Glover, “One-loop helicity amplitudes for  $H \rightarrow$  gluons: The All-minus configuration,” *Nucl.Phys.Proc.Suppl.* **160** (2006) 71–75, [hep-ph/0607139](#).
- [30] S. Badger, E. N. Glover, and K. Risager, “One-loop phi-MHV amplitudes using the unitarity bootstrap,” *JHEP* **0707** (2007) 066, [0704.3914](#).
- [31] E. N. Glover, P. Mastrolia, and C. Williams, “One-loop phi-MHV amplitudes using the unitarity bootstrap: The General helicity case,” *JHEP* **0808** (2008) 017, [0804.4149](#).
- [32] S. Badger, E. Nigel Glover, P. Mastrolia, and C. Williams, “One-loop Higgs plus four gluon amplitudes: Full analytic results,” *JHEP* **1001** (2010) 036, [0909.4475](#).
- [33] L. J. Dixon and Y. Sofianatos, “Analytic one-loop amplitudes for a Higgs boson plus four partons,” *JHEP* **0908** (2009) 058, [0906.0008](#).
- [34] S. Badger, J. M. Campbell, R. K. Ellis, and C. Williams, “Analytic results for the one-loop NMHV Hqgg amplitude,” *JHEP* **0912** (2009) 035, [0910.4481](#).
- [35] J. M. Campbell, R. K. Ellis, R. Frederix, P. Nason, C. Oleari, *et al.*, “NLO Higgs Boson Production Plus One and Two Jets Using the POWHEG BOX, MadGraph4 and MCFM,” *JHEP* **1207** (2012) 092, [1202.5475](#).
- [36] T. Binoth, F. Boudjema, G. Dissertori, A. Lazopoulos, A. Denner, *et al.*, “A Proposal for a standard interface between Monte Carlo tools and one-loop programs,” *Comput.Phys.Comm.* **181** (2010) 1612–1622, [1001.1307](#). Dedicated to the memory of, and in tribute to, Thomas Binoth, who led the effort to develop this proposal for Les Houches 2009.
- [37] G. Cullen, N. Greiner, G. Heinrich, G. Luisoni, P. Mastrolia, *et al.*, “Automated One-Loop Calculations with GoSam,” *Eur.Phys.J.* **C72** (2012) 1889, [1111.2034](#).
- [38] T. Gleisberg, S. Hoeche, F. Krauss, M. Schonherr, S. Schumann, *et al.*, “Event generation with SHERPA 1.1,” *JHEP* **0902** (2009) 007, [0811.4622](#).
- [39] G. Luisoni, M. Schönerr, and F. Tramontano, in preparation.
- [40] <http://gosam.hepforge.org/proc/>.
- [41] G. Ossola, C. G. Papadopoulos, and R. Pittau, “Reducing full one-loop amplitudes to scalar integrals at the integrand level,” *Nucl.Phys.* **B763** (2007) 147–169, [hep-ph/0609007](#).
- [42] G. Ossola, C. G. Papadopoulos, and R. Pittau, “Numerical evaluation of six-photon amplitudes,” *JHEP* **0707** (2007) 085, [0704.1271](#).
- [43] R. K. Ellis, W. T. Giele, and Z. Kunszt, “A Numerical Unitarity Formalism for Evaluating One-Loop Amplitudes,” *JHEP* **03** (2008) 003, [0708.2398](#).
- [44] W. T. Giele, Z. Kunszt, and K. Melnikov, “Full one-loop amplitudes from tree amplitudes,” *JHEP* **0804** (2008) 049, [0801.2237](#).
- [45] P. Mastrolia, G. Ossola, T. Reiter, and F. Tramontano, “Scattering Amplitudes from Unitarity-based Reduction Algorithm at the Integrand-level,” *JHEP* **1008** (2010) 080, [1006.0710](#).
- [46] P. Mastrolia, E. Mirabella, G. Ossola, and T. Peraro, “Scattering Amplitudes from Multivariate Polynomial Division,” *Phys.Lett.* **B718** (2012) 173–177, [1205.7087](#).
- [47] P. Mastrolia, E. Mirabella, and T. Peraro, “Integrand reduction of one-loop scattering amplitudes through Laurent series expansion,” [1203.0291](#).
- [48] P. Nogueira, “Automatic Feynman graph generation,” *J.Comput.Phys.* **105** (1993) 279–289.
- [49] J. A. M. Vermaseren, “New features of FORM,” [math-ph/0010025](#).
- [50] T. Reiter, “Optimising Code Generation with haggies,” *Comput.Phys.Comm.* **181** (2010) 1301–1331, [0907.3714](#).
- [51] G. Cullen, M. Koch-Janusz, and T. Reiter, “Spinney: A Form Library for Helicity Spinors,” *Comput.Phys.Comm.* **182** (2011) 2368–2387, [1008.0803](#).
- [52] G. Ossola, C. G. Papadopoulos, and R. Pittau, “On the Rational Terms of the one-loop amplitudes,” *JHEP* **0805** (2008) 004, [0802.1876](#).
- [53] P. Mastrolia, G. Ossola, C. Papadopoulos, and R. Pittau, “Optimizing the Reduction of One-Loop Amplitudes,” *JHEP* **0806** (2008) 030, [0803.3964](#).
- [54] G. Heinrich, G. Ossola, T. Reiter, and F. Tramontano, “Tensorial Reconstruction at the Integrand Level,” *JHEP* **1010** (2010) 105, [1008.2441](#).
- [55] G. van Oldenborgh, “FF: A Package to evaluate one loop Feynman diagrams,” *Comput.Phys.Comm.* **66** (1991) 1–15.
- [56] R. K. Ellis and G. Zanderighi, “Scalar one-loop integrals for QCD,” *JHEP* **02** (2008) 002, [0712.1851](#).
- [57] A. van Hameren, “OneLOop: For the evaluation of one-loop scalar functions,” *Comput.Phys.Comm.* **182** (2011) 2427–2438, [1007.4716](#).
- [58] G. Cullen, J. Guillet, G. Heinrich, T. Kleinschmidt, E. Pilon, *et al.*, “Golem95C: A library for one-loop integrals with complex masses,” *Comput.Phys.Comm.* **182** (2011) 2276–2284, [1101.5595](#).
- [59] F. Krauss, R. Kuhn, and G. Soff, “AMEGIC++ 1.0: A Matrix element generator in C++,” *JHEP* **0202** (2002) 044, [hep-ph/0109036](#).
- [60] T. Gleisberg and F. Krauss, “Automating dipole subtraction for QCD NLO calculations,” *Eur.Phys.J.* **C53** (2008) 501–523, [0709.2881](#).
- [61] W. Giele and E. N. Glover, “Higher order corrections to jet cross-sections in  $e^+e^-$  annihilation,” *Phys.Rev.* **D46** (1992) 1980–2010.
- [62] Z. Kunszt, A. Signer, and Z. Trocsanyi, “Singular terms of helicity amplitudes at one loop in QCD and the soft limit of the cross-sections of multiparton processes,” *Nucl.Phys.* **B420** (1994) 550–564, [hep-ph/9401294](#).
- [63] S. Catani and M. Seymour, “The Dipole formalism for the calculation of QCD jet cross-sections at next-to-leading order,” *Phys.Lett.* **B378** (1996) 287–301, [hep-ph/9602277](#).
- [64] S. Catani and M. Seymour, “A General algorithm for calculating jet cross-sections in NLO QCD,” *Nucl.Phys.* **B485** (1997) 291–419, [hep-ph/9605323](#).
- [65] S. Catani, S. Dittmaier, and Z. Trocsanyi, “One loop singular behavior of QCD and SUSY QCD amplitudes with massive partons,” *Phys.Lett.* **B500** (2001) 149–160, [hep-ph/0011222](#).
- [66] S. Hoeche, F. Krauss, M. Schonherr, and F. Siegert, “QCD matrix elements + parton showers: The NLO case,” [1207.5030](#).
- [67] SHERPA collaboration, in preparation.
- [68] J. Pumplin, D. Stump, J. Huston, H. Lai, P. M. Nadolsky, *et al.*, “New generation of parton distributions with uncertainties from global QCD analysis,” *JHEP* **0207** (2002) 012, [hep-ph/0201195](#).
- [69] M. Cacciari and G. P. Salam, “Dispelling the  $N^3$  myth for the  $k_t$  jet-finder,” *Phys.Lett.* **B641** (2006) 57–61, [hep-ph/0512210](#).
- [70] M. Cacciari, G. P. Salam, and G. Soyez, “The Anti- $k(t)$  jet clustering algorithm,” *JHEP* **0804** (2008) 063, [0802.1189](#).
- [71] M. Cacciari, G. P. Salam, and G. Soyez, “FastJet User Manual,” *Eur.Phys.J.* **C72** (2012) 1896, [1111.6097](#).
- [72] T. Hahn, “Generating Feynman diagrams and amplitudes with FeynArts 3,” *Comput.Phys.Comm.* **140** (2001) 418–431, [hep-ph/0012260](#).